Low Fidelity Multidisciplinary Methodology for Efficient and Quiet Propeller Design Numerical Investigation and Experimental Validation

Margalida, G.; della Corte, B.; Sinnige, T.; Knepper, Kylie ; Soemarwoto, Bambang; Nahuis, Ruben

DOI
10.2514/6.2024-3317

Publication date
2024

Document Version
Final published version

Published in
30th AIAA/CEAS Aeroacoustics Conference (2024)

Aeroacoustics Conferences
June 4-7, 2024, Rome, Italy
30th AIAA/CEAS Aeroacoustics Conference (2024)

10.2514/6.2024-3317

Low fidelity multidisciplinary methodology for efficient and quiet propeller design: Numerical investigation and experimental validation

Gabriel Margalida[1], Biagio della Corte[2] and Tomas Sinnige[3]

Delft University of Technology, Delft, 2629 HS, The Netherland

Kylie Knepper[4], Bambang Soemarwoto[5] and Ruben Nahuis[6]

Royal Netherlands Aerospace Centre NLR, Amsterdam, 1059 CM, The Netherlands

This paper discusses the early-stage development of a fast propeller design tool using low-fidelity methods. Aerodynamics, aeroacoustics, and structural behavior of the propeller have been incorporated into an optimization framework to generate more efficient and quieter propeller designs. A first optimization process has successfully provided a set of more efficient and/or quieter designs among which one specific geometry has been manufactured. CFD validation has confirmed its aerodynamic performances and reasonable agreements have been observed with experimental results, with some discrepancies, however. Additional parametric studies are also discussed.

Nomenclature

β	=	Blade pitch angle (°)	f_{out}	=	Objective function optimum value
BPF	=	Blade passing frequency	γ	=	Twist angle (°)
c_i/ceq_i	=	Equality/inequality constraint	M	=	Mach number
$c_{in.}/c_{out.}$	=	Mean chord length inboard/outboard	t_j	=	Duration ratio
D	=	Propeller diameter	Q	=	Torque (Nm)
C_T	=	Thrust coefficient, $T/(\rho.f_P^2.D^4)$	R_p	=	Propeller radius (m)
C_P	=	Power coefficient, $T/(\rho.f_P^3.D^5)$	T	=	Thrust (N)
J	=	Advance ratio, $U_\infty/(2.f_P.R_P)$	U_∞	=	Freedtream velocity ($m.s^{-1}$)
f_P	=	Propeller rotational frequency	x_i	=	Optimization input vector
η	=	Propeller efficiency	xl_i / xu_i	=	Input vector lower/upper bounds
f	=	Objective function	x_{out}	=	Output optimized vector

[1] Research Associate, Faculty of Aerospace Engineering, Flight Performance and Propulsion,
[2] Research Associate, Faculty of Aerospace Engineering, Flight Performance and Propulsion,
[3] Assistant professor, Faculty of Aerospace Engineering, Flight Performance and Propulsion,
[4] R&D Engineer Aeroacoustics, Vertical Flight & Aeroacoustics Dept
[5] R&D Engineer Aeroacoustics, Vertical Flight & Aeroacoustics Dept
[6] R&D Engineer Aeroacoustics, Vertical Flight & Aeroacoustics Dept

I. Introduction

Rapid acceleration of climate change and its alarming repercussions on the environment have led to increasingly stringent regulations across all sectors, and the aviation industry is facing growing scrutiny and social defiance. Simultaneously, a surge in the number of electrically propelled aircraft developments, spanning from fully electric to hydrogen-electric models, has been witnessed. The momentum has shifted dramatically, from a steady 25% annual increase until 2016 to 50% since [1]. This electrification, initially dominated by urban air mobility and general aviation, has now extended to regional and large commercial aircraft, driven by industry giants and innovative startups alike.

This proliferation in aircraft initiatives introduces a myriad of flight conditions and diverse configurations, and incorporating all these variables as early in the design phase as possible has become even more important. Hence, the need for a holistic approach, especially in the context of propeller design and integration, necessitates the development of a versatile and fast design tool capable of providing optimized blade geometries and enabling designers to optimize propellers for efficient and quiet operations across a spectrum of applications.

Moreover, in the quest for more sustainable aviation solutions, propellers are regaining attention as their efficiency presents a compelling case for reconsideration. However, addressing the historical obstacle of noise remains a critical aspect.

This paper will discuss the early-stage development of a fast propeller design tool using low-fidelity methods. Aerodynamics, aeroacoustics, and structural behavior of the propeller have been incorporated into an optimization framework to generate more efficient and quieter propeller designs. The performance of those designs has then been verified using higher fidelity methods, before being tested during two wind tunnel test campaigns. The main enablers of noise and power requirement reduction are also discussed in this study as well as the limitations encountered with the current implementation of the tool.

II. Methodology and set-up

The reference propeller for this study is the XPROP propeller, originally designed for a regional turboprop with similar specifications as the ATR42/72 family. A model scale propeller geometry, tested in previous projects [2], [3], [4], has been used as a reference point. This propeller features 6 carbon fiber blades and a diameter of 0.4064m.

The noise/aerodynamic optimization, with inherently conflicting objectives, has been treated sequentially as single objective problems using a gradient-based method (SQP algorithm). One objective is optimized while the other is constrained (ε-method). For this study, the propeller is firstly optimized to minimize the power requirement (D_0 to D_1 on Fig. 1.(a)), at the expense of the noise performances. A Pareto front is then generated through several consecutive optimizations (D_1 to D_i on Fig. 1.(a)), where the noise is minimized while the power requirement constrained to the previous design value with an additional penalty.

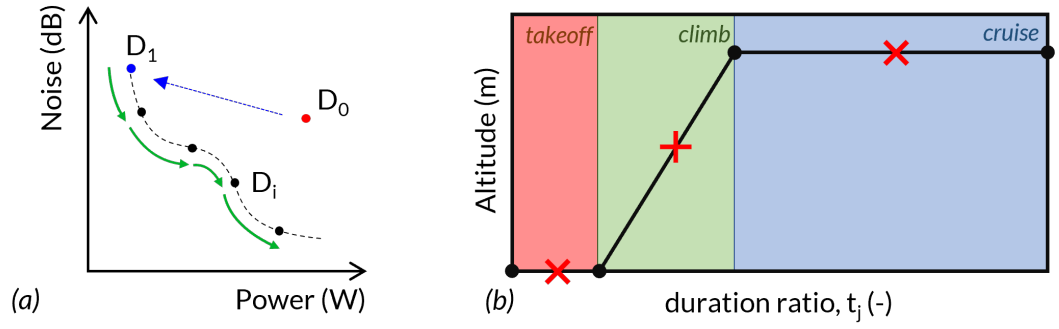

Fig. 1 Optimization methodology. Pareto front generation (a), flight profile example (b)

Moreover, each objective is computed over a generic flight profile, including 3 phases, take-off, climb and cruise, as depicted in Fig. 1.(b). The value of the power, noise respectively, is thus computed for each phase (takeoff and climb only for noise), and then weighted by the time spent in the corresponding phase and averaged.

The optimization workflow is articulated around several "building blocks" embedded in a global tool which makes the link from one solver to the other. This workflow, schematized in Fig. 2, incorporates:

i. a blade designer, using a stack of 2D airfoils to generate a 3D blade. Each section is defined by a set of parameters controlled by several Bézier curves describing their distribution along the blade span.
ii. a propeller/wake generator (geometrical and operational) to define the propeller and its semi-free wake [5].
iii. an aerodynamic solver based on a modern implementation of the Lifting Line Theory [6] (LLT) with several corrections [7], [8] to evaluate the blade local aerodynamic forces and consequently the performances of the propeller (Thrust/Torque).
iv. an acoustic solver, developed by Goyal [9], based on Hanson's Helicoidal Surface Theory (HST) [10] to evaluate the noise directivity level.
v. a structural solver based on Euler-Bernoulli Beam Theory (EBBT) [11] to evaluate the blade stress, deflection, and torsion.

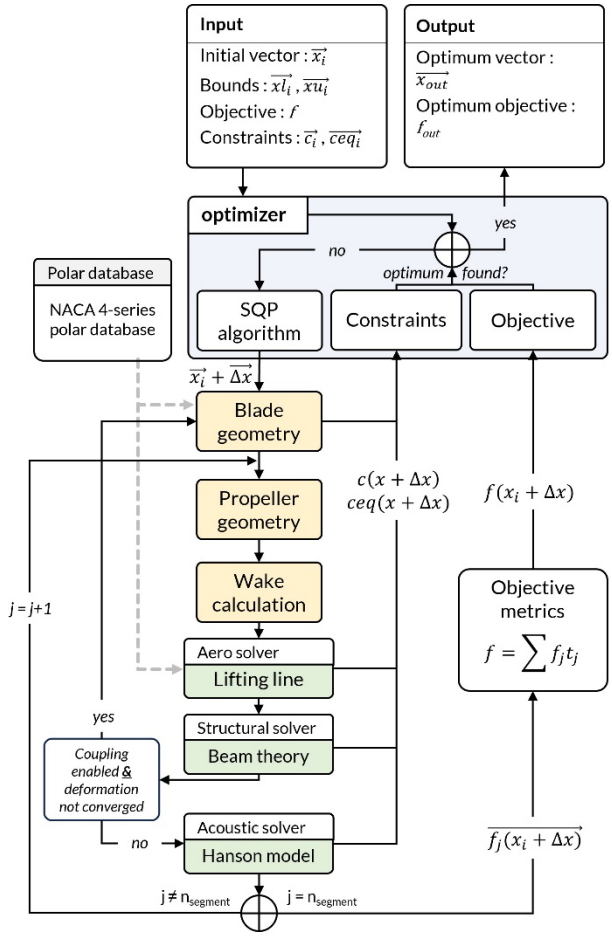

Fig. 2 Optimization workflow

The resulting optimized blade geometry has then been compared to RANS CFD for the same three flight conditions used during optimization (take-off, climb and cruise).

Finally, the reference propeller and the optimized propeller have been manufactured and tested during two experimental campaigns. Acoustic measurements have been conducted at the Aeroacoustic Wind Tunnel (AWT) of NLR Marknesse using TUD propeller test rig and a linear array of 10 microphones. Several blade pitch angles and rotational speeds have been tested for Mach numbers ranging from 0.09 to 0.15. Aerodynamic performances have been measured at the Low Turbulence Wind Tunnel (LTT) of TU Delft using the same propellers, test rig and conditions (Mach number, pitch, rotational speed).

During the manufacturing process, additional numerical studies have been done using different geometrical parameters and conditions, and with some modifications to the models. The results of those studies are also discussed in this paper.

III. Results

From the first optimization process, a Pareto front of optimum designs has been successfully generated, as depicted in Fig. 3. A blade geometry providing noise and power requirement reduction, as predicted by the low-fidelity toolchain, has been selected along this Pareto front. This geometry, named S2PROP, has then be verified using RANS CFD (see right plot of Fig. 2) and has confirmed its better noise and aerodynamic performances compared to XPROP.

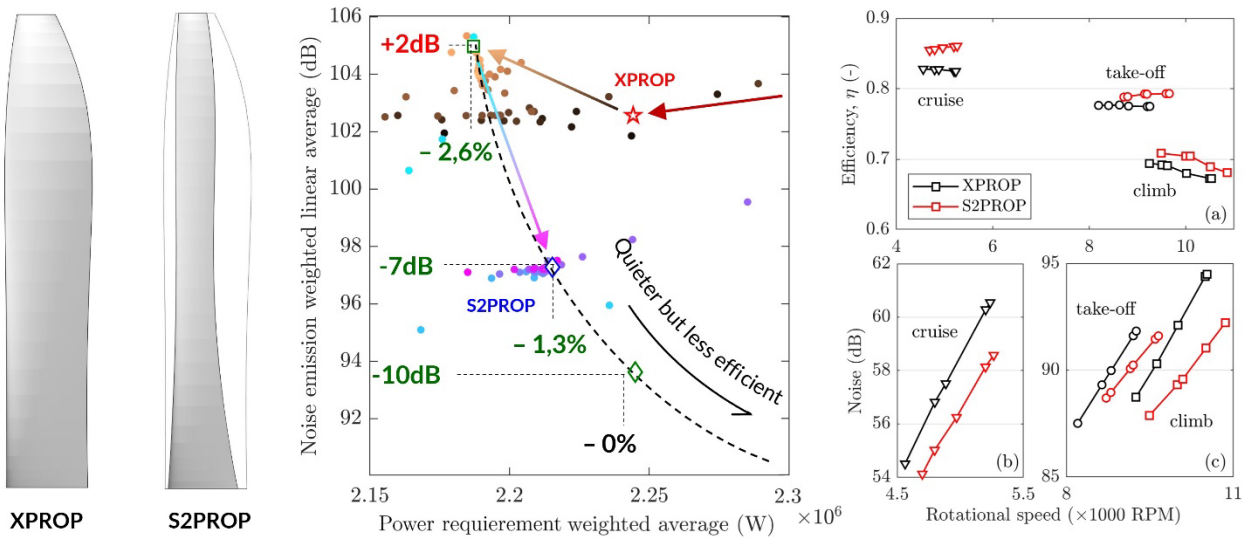

Fig. 3 Optimization output. Initial / selected blade design (left), noise / aerodynamic performances map (center), CFD validation (right)

The experimental validation of S2PROP aerodynamic performances is however more nuanced, as it can be seen on Fig. 4. For the thrust coefficient first, as the advance ratio increases, the model tends to overpredict the thrust more. This behavior is most likely due to the low Reynolds number, around 50.000, experienced for those conditions (low rotational speed and small chord length). Under such low Reynolds numbers, the laminar/turbulent transition prediction is critical and will strongly affect lift/drag coefficient estimation (respectively C_L and C_D). A misprediction of this transition is likely to be the cause of the observed deviation. By contrast, the performance predictions of the XPROP propeller, featuring a wider chord, align more closely with the experimental measurements, as depicted in Fig. 5.

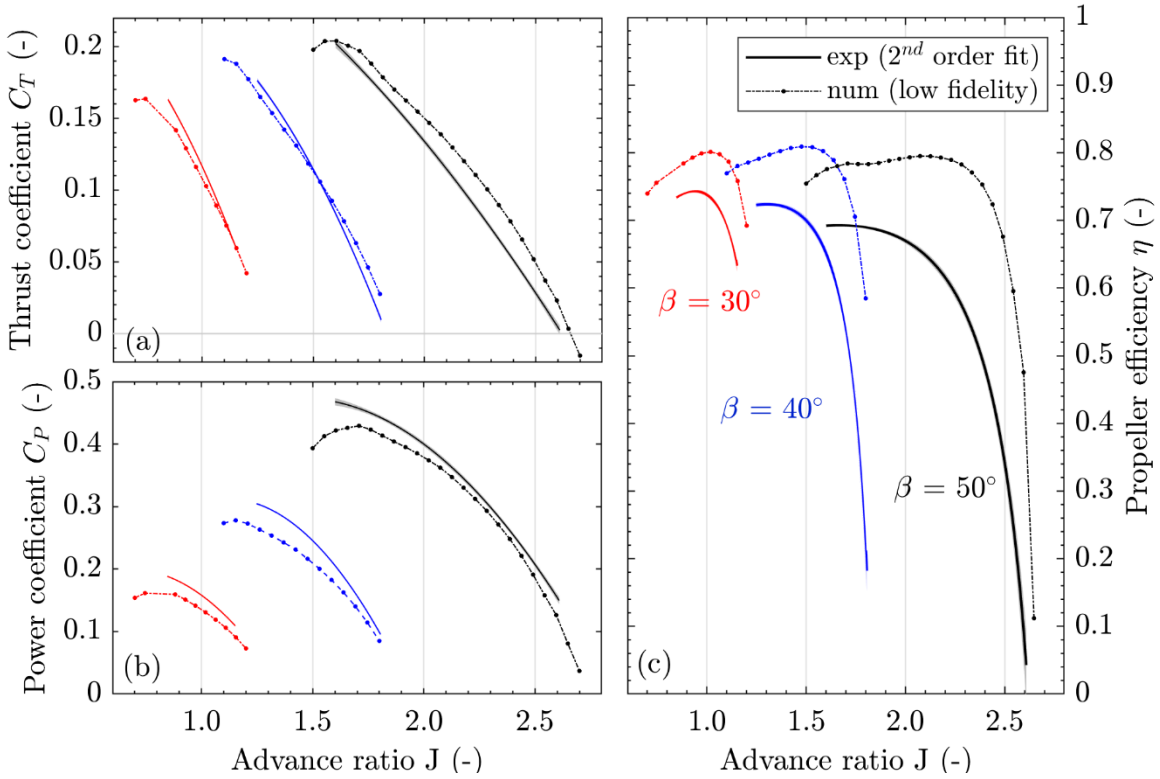

Fig. 4 Aerodynamic performances of S2PROP propeller. Thrust coefficient (a), Power coefficient (b) and propeller efficiency (c) vs advance ratio for three pitch settings ($\beta_{0.7R}$ = [30°, 40°, 50°]). M=0.12, symmetric flow conditions

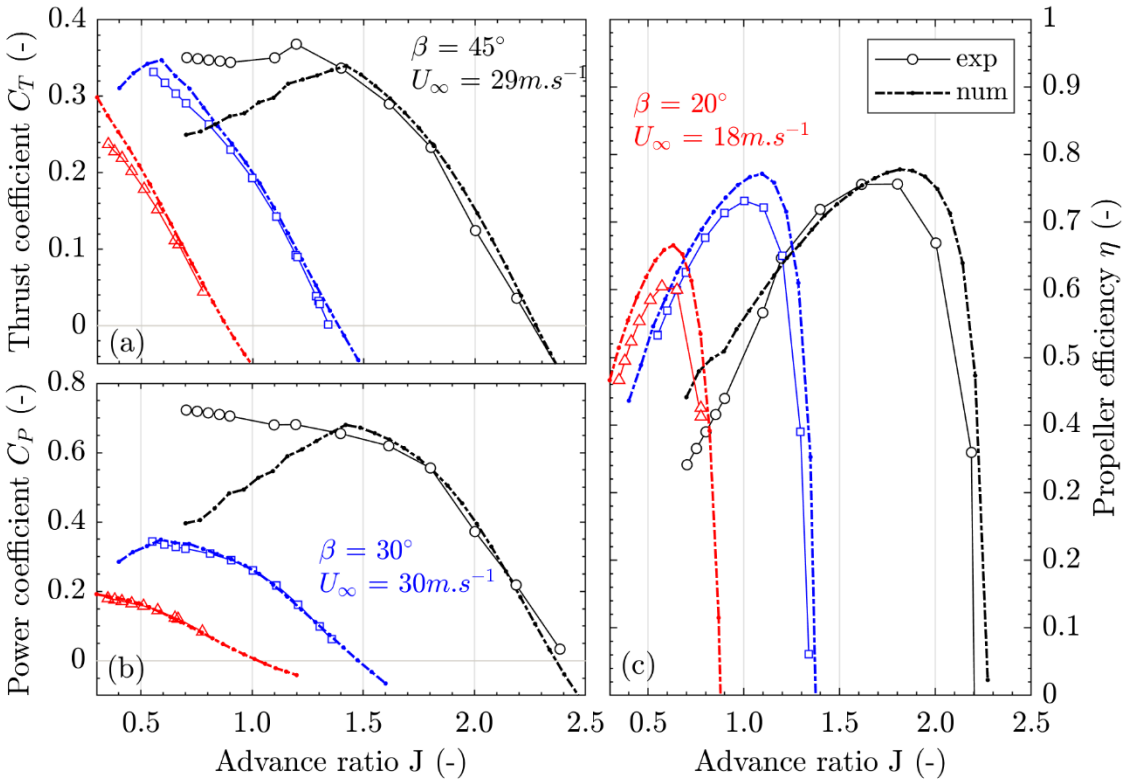

Fig. 5 Aerodynamic performances of XPROP propeller. Thrust coefficient (a), Power coefficient (b) and propeller efficiency (c) vs advance ratio for three pitch settings (β0.7R = [20°, 30°, 45°] and M=[0.055, 0.087, 0.085]). Symmetric flow conditions

For the torque, the opposite behavior is observed, as the advance ratio decreases, the underprediction of the torque increases. One could expect the torque to follow the same trend as the thrust, because if C_L is overpredicted, C_D should be underpredicted. However, for a given inflow angle (given advance ratio), if the lift is overpredicted, thrust and torque both end up being overpredicted by the same amount. This overprediction of the torque, due to C_L, then balances the underprediction of the torque due to C_D. As a result, the propeller efficiency is overpredicted by about the same amount, ~10%, over the entire advance ratio range.

The propeller and microphone setup are presented in Fig. 6 and Table 1. Some of the noise directivity patterns of the S2PROP propeller are displayed for different pitch setting β, Mach number M and advance ratio J, in Fig. 7. In the context of the optimization framework presented in this paper, we are more interested in the relative reduction of the noise emissions from one condition to the other because it is how the optimizer determines the search direction. The evolution of the maximum SPL, with respect to the maximum SPL measured at the lowest advance ratio of a given pitch setting, is displayed in Fig. 8 for the experimental measurements and the predicted numerical values.

Table 1 Microphones location

Mic #	x/R$_P$	y/R$_P$	z/R$_P$	d/R$_P$	Θ (°)
1	–5.49			–11.28	61
2	–3.59			–10.48	70
3	–1.74			–10.00	80
4	0			–9.85	90
5	1.74	–9.85	0	–10.00	100
6	3.59			–10.48	110
7	5.49			–11.28	119
8	8.27			–12.86	130
9	11.74			–15.33	140
10	0	+9.85		+9.85	270

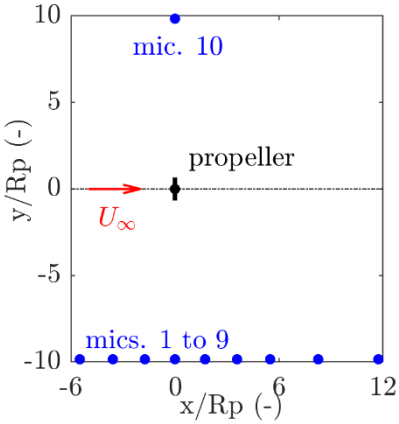

Fig. 6 Microphones setup

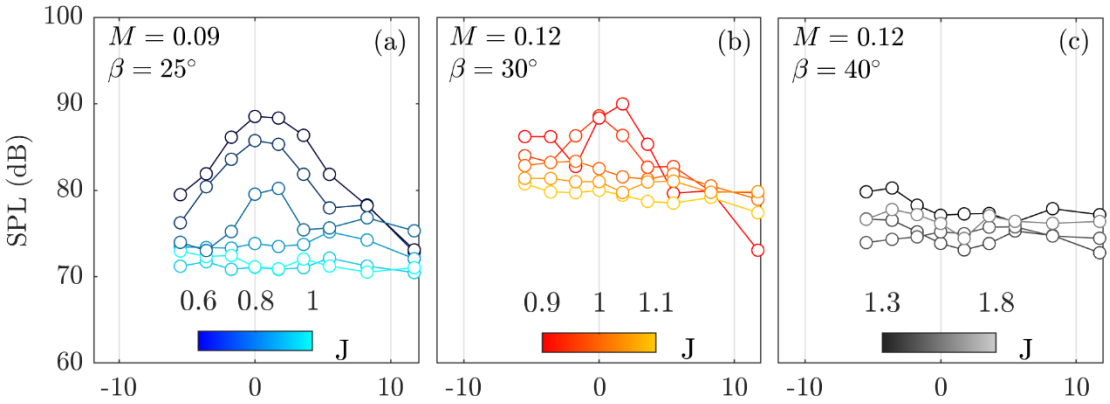

Fig. 7 Noise directivity of S2PROP propeller. Advance ratio sweep J ∈ [0.6 ; 1], 25° pitch and Mach 0.09 (a), advance ratio sweep J ∈ [0.9 ; 1.1], 30° pitch and Mach 0.12 (b), advance ratio sweep J ∈ [1.3 ; 1.8], 40° pitch and Mach 0.12

Of all the conditions analyzed, only the 25° pitch setting running at Mach 0.09, displayed in Fig. 7.(a), exhibits enough tonal content to assess this point. Indeed, the directivity plot for the lowest advance ratio shows a decrease of the maximum sound pressure level (SPL) in the propeller plane region before reaching a plateau. When the SPL is mostly tonal, the decrease of its amplitude in the propeller plane region matches the predicted decrease by the solver. However, as soon as the broadband noise becomes dominant the trends diverge, as visible for the pitch setting β=30° and β=40° in Fig. 8.

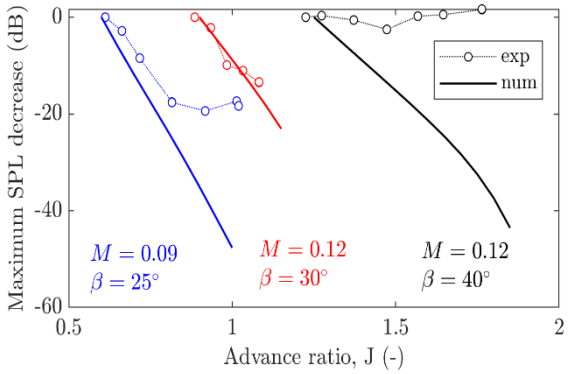

Fig. 8 Maximum SPL reduction of S2PROP propeller (w.r.t. lowest advance ratio SPL)

As outlined above, the lobe visible in the propeller plane disappears for lower advance ratio. For those rotational speed, the broadband noise becomes dominant over the tonal noise. Because the broadband noise isn't resolved in the present model, the directivity plot continues decreasing. Including broadband noise is thus essential to obtain accurate results at lower tip Mach number and local Reynolds number.

As mentioned at the end of previous section, several sensitivity studies have been conducted during the manufacturing of the selected blade design S2PROP. An overview of the results from these analyses is presented in Fig. 9 to Fig. 11. As a reminder, D_1 is obtained from D_0 by optimizing the chord, twist, advance ratio, and pitch for the aerodynamic objective and then D_2 to D_6 from D_1 by optimizing for the noise objective with a constraint on the aerodynamic penalty. This full optimization process is later referred as 4p-optimization and is represented by black colors in Fig. 9 to Fig. 11. Points d_2 to d_5 follow the same methodology with only the advance ratio and pitch being optimized. This process is referred as 2p-optimization in the following and represented in green.

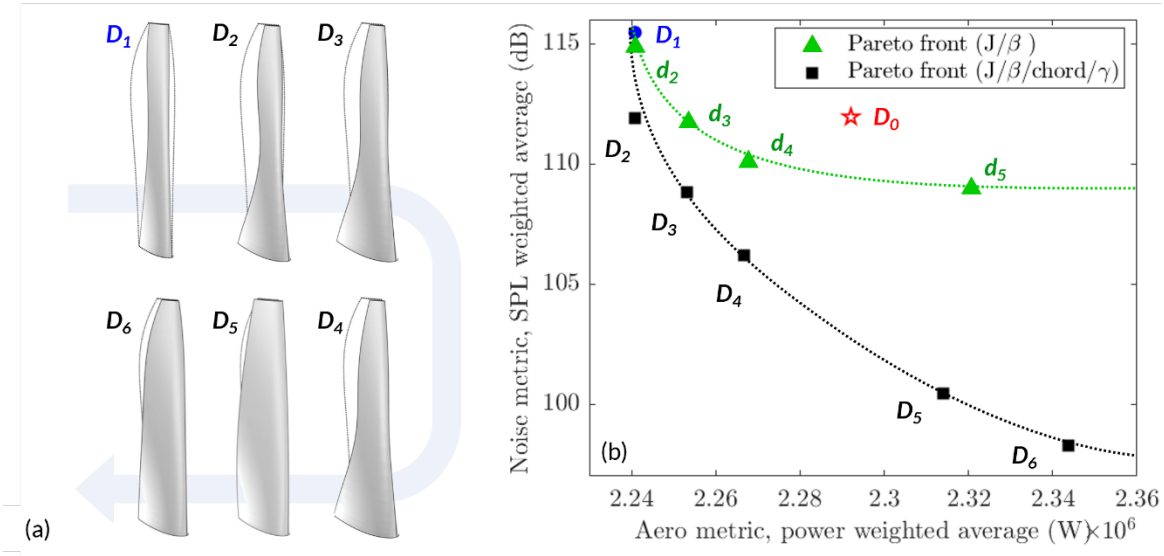

Fig. 9 Blade shape optimization (chord c, twist γ, advance ratio J, pitch β) pareto front. Blade geometries (a), noise/aerodynamic performances (b)

For the 2p-optimization, the only usable lever to reduce the noise is the advance ratio. By doing so, all components of the noise are reduced (thickness and loading). Consequently, the optimizer increases the pitch, as visible on Fig. 10.(c) to balance the thrust decrease generated by the rotational speed reduction.

For the 4p-optimization, it appears that the trends are similar and that the main source of noise reduction is obtained thanks to a lower rotational speed. However, the optimizer is able to decrease the rotational speed further (Fig. 10.(d)), while maintaining the same pitch range (Fig. 10.(c)), hence giving access to more noise reduction, as visible on Fig. 10.(a). This increased range of rpm reduction is possible because of the additional parameters the optimizer has access to. As depicted inFig. 11.(b), the chord steadily increases all along the span of the blade, hence generating more lift and thus requiring less speed. It can also be seen that the optimizer starts increasing the chord firstly toward the hub while maintaining a narrow tip (logarithm trend for $c_{in.}$ and exponential trend for $c_{out.}$, Fig. 11.(b)) in order to keep smaller chord length in the fast-moving part of the blade.

On Fig. 11.(c)) it can be seen that the twist distribution is also modified, with a significant increase of the twist in the outboard part of the blade (increase in the negative direction). This has a direct effect on the thrust distribution which remains lower outboard for all geometries (D_2 to D_6) compared to D_0, thus reducing the loading noise. From this first analysis, the advance ratio (rotational speed) appears to be the main key to propeller noise reduction, affecting all the types of tonal

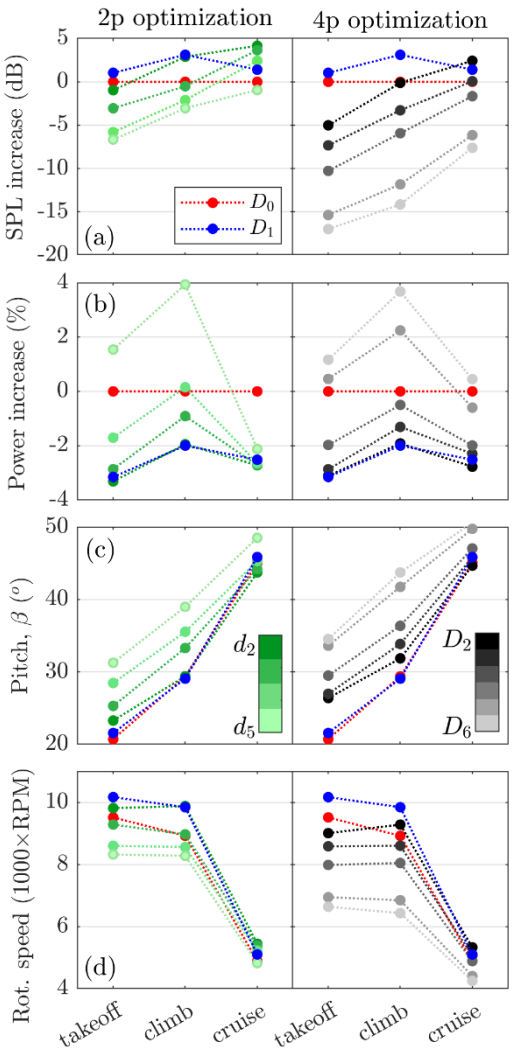

Fig. 10 Operational conditions along the Pareto fronts at each flight phase. Noise increase (a) and power increase (b) w.r.t. D_0, blade pitch (c), propeller

noise sources. Decreasing the chord grants access to larger advance ratio and changing the chord and twist distribution helps moving the loading inboard, where the local Mach number is lower.

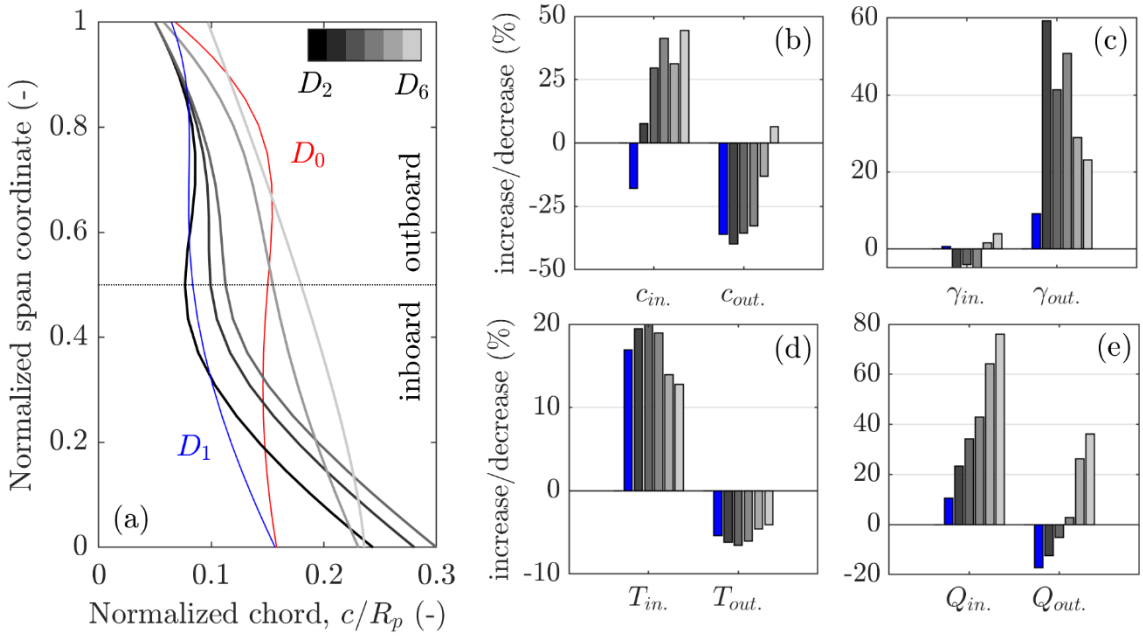

Fig. 11 Geometrical parameters and blade local force evolution along the Pareto front. Spanwise chord distribution (a), inboard/outboard mean chord/twist evolution w.r.t. D_0 (b-c), inboard/outboard thrust/torque evolution during climb w.r.t. D_0 (d-e)

The total tonal noise directivity and the different contributions are displayed in Fig. 12. Overall, from D_1 to D_6, all components are decreasing because the rotational speed decreases. However, it is worth noting the influence of the blade shape on the noise directivity. From D_1 to D_2 and from D_2 to D_3 for example, the rotational speed decreases by the same amount during climb (see Fig. 10.(d)), however, the decrease of the thickness noise is much more pronounced from D_1 to D_2 (see, Fig. 12.(b), -8.8dB and -1.6dB respectively). The main difference between those cases is the chord length distribution. Indeed, the chord length decreases by 20% close to the tip of the blade (Fig. 11.(a)) from D_1 to D_2 and remain the same from D_2 to D_3, while increasing in both cases by 25% in the inboard half of the blade. The chord reduction outboard hence provides a bigger noise decrease.

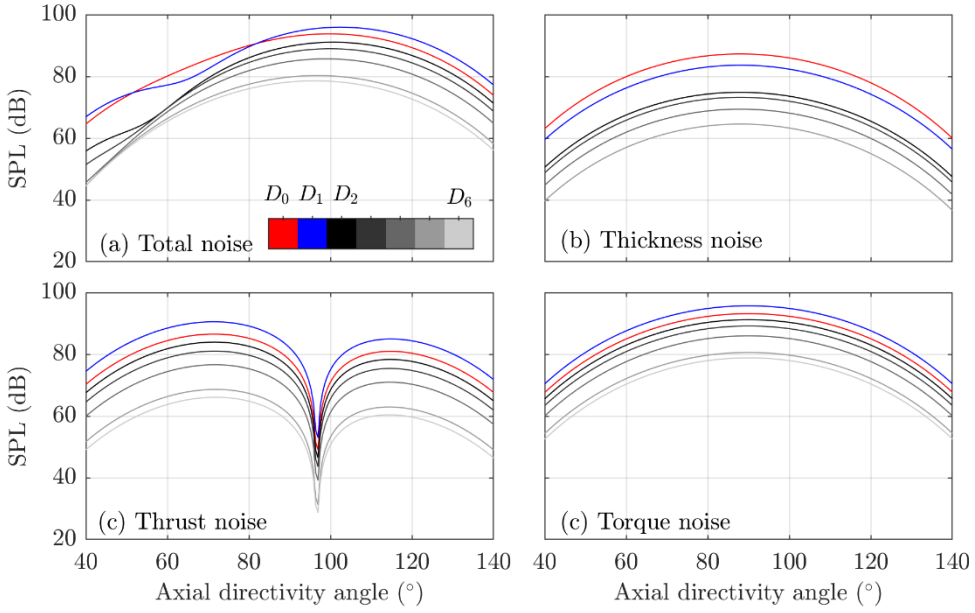

Fig. 12 Tonal noise directivity during climb along the 4p-optimization pareto front. Total noise (a), thickness noise (b), thrust noise (c) and torque noise (d)

This modification of the blade shape also causes a redistribution of the thrust (Fig. 11d)) granting the same reduction of the thrust noise (see, Fig. 12.(c)). Further down along the pareto front, the chord increases all over the span of the blade (Fig. 11.(a)) but it is then counterbalanced by a large reduction of the rotational speed (see Fig. 10.(d)).

From D_0 to D_6, the torque noise remains the main contributor to the overall noise and doesn't decrease as much as the other components. Indeed, regardless the optimization goal, the torque is influenced by competing parameters. When the optimizer has to reduce the total energy consumption, it will decrease the chord length, hence the torque and its associated noise, but must compensate to maintain the thrust requirement by increasing the rotational speed, and by doing so, all noise contributions, including torque noise, increase.

IV. Conclusion

In this study, the blade designs obtained with the use of a fast optimization framework and low-fidelity models have been analyzed.

A first design, named S2PROP, has been built and validated using RANS CFD and two experimental campaigns. The numerical simulation has shown the improvement of both the aerodynamic and acoustic performances of the new design for a specific flight path, composed of a take-off, climb and cruise segment. The experimental validation has outlined more nuanced results, mainly due to the limitations inherent to the small chord length and tip Mach number (small local Reynolds number). Indeed, a significant misprediction of the torque of the propeller has been observed (leading to an overestimated efficiency compared to measured performances). In addition, the propeller has shown to be dominated by broadband noise on a large range of advance ratio and pitch settings, leading to some difficulties to validate the noise directivity predictions. However, both for the aerodynamic or for the acoustics predictions, the trends of the physical quantities are correctly predicted, and thus, doesn't invalidate the results and global behavior of the optimization.

The different optimizations have highlighted that the main parameter enabling noise reduction (for a fixed number of blade and a given thrust) is the rotational speed because it affects all the components of the sound through the reduction of the tip Mach number. Then the optimizer uses the other parameters (the more the better) available to minimize the noise emission while maintaining the required thrust. Finally, it has also been shown that more subtle changes of the blade shape can also enable greater noise reduction by redistributing the loading inboard, where the local sections move at lower Mach number.

V. Acknowledgments

The research in this paper is part of the Smart Rotors project, supported by the European Union under the "Kansen voor West 2" program for regional development.

The authors would like to express special thanks to Stevie Janssen (NLR) and Harry Brouwer (NLR) who actively participated in regular meetings about tool development and optimization setup, providing valuable insights, and whose contributions have helped shaping the overall direction of this work.

VI. References

[1] Thomson Robert, "Electric propulsion is finally on the map," https://www.rolandberger.com/en/Insights/Publications/Electric-propulsion-is-finally-on-the-map.html.

[2] T. C. A. Stokkermans and L. L. M. Veldhuis, “Propeller Performance at Large Angle of Attack Applicable to Compound Helicopters,” *AIAA Journal*, vol. 59, no. 6, pp. 2183–2199, Jun. 2021, doi: 10.2514/1.J059509.

[3] N. v. Arnhem, R. Vos, and L. L. Veldhuis, “Aerodynamic Loads on an Aft-Mounted Propeller Induced by the Wing Wake,” in *AIAA Scitech 2019 Forum*, Reston, Virginia: American Institute of Aeronautics and Astronautics, Jan. 2019. doi: 10.2514/6.2019-1093.

[4] Q. Li *et al.*, “Design and Experimental Validation of Swirl-Recovery Vanes for Propeller Propulsion Systems,” *AIAA Journal*, vol. 56, no. 12, pp. 4719–4729, Dec. 2018, doi: 10.2514/1.J057113.

[5] W. Khan and M. Nahon, “Improvement and validation of a propeller slipstream model for small unmanned aerial vehicles,” in *2014 International Conference on Unmanned Aircraft Systems (ICUAS)*, IEEE, May 2014, pp. 808–814. doi: 10.1109/ICUAS.2014.6842326.

[6] W. F. Phillips and D. O. Snyder, “Modern adaptation of Prandtl’s classic lifting-line theory,” *J Aircr*, vol. 37, no. 4, pp. 662–670, 2000, doi: 10.2514/2.2649.

[7] C. D. Goates and D. F. Hunsaker, “Practical Implementation of a General Numerical Lifting-Line Method,” in *AIAA Scitech 2021 Forum*, Reston, Virginia: American Institute of Aeronautics and Astronautics, Jan. 2021. doi: 10.2514/6.2021-0118.

[8] D. Küchemann, “A simple method for calculating the span and chordwise loading on straight and swept wings of any given aspect ratio at subsonic speeds,” 1952.

[9] J. Goyal, “Hanson’s Model in Frequency Domain - Tonal Noise of Rotors in Uniform Inflow.” 4TU.ResearchData. software, 2024.

[10] D. B. Hanson, “Helicoidal Surface Theory for Harmonic Noise of Propellers in the Far Field,” vol. 18, no. 10, 1980.

[11] J. Sodja, R. Drazumeric, T. Kosel, and P. Marzocca, “Design of Flexible Propellers with Optimized Load-Distribution Characteristics,” *J Aircr*, vol. 51, no. 1, pp. 117–128, Jan. 2014, doi: 10.2514/1.C032131.